Volume 6 | Number 12 | December 2019 | Pages 3483–3746

Environmental Science Nano

rsc.li/es-nano

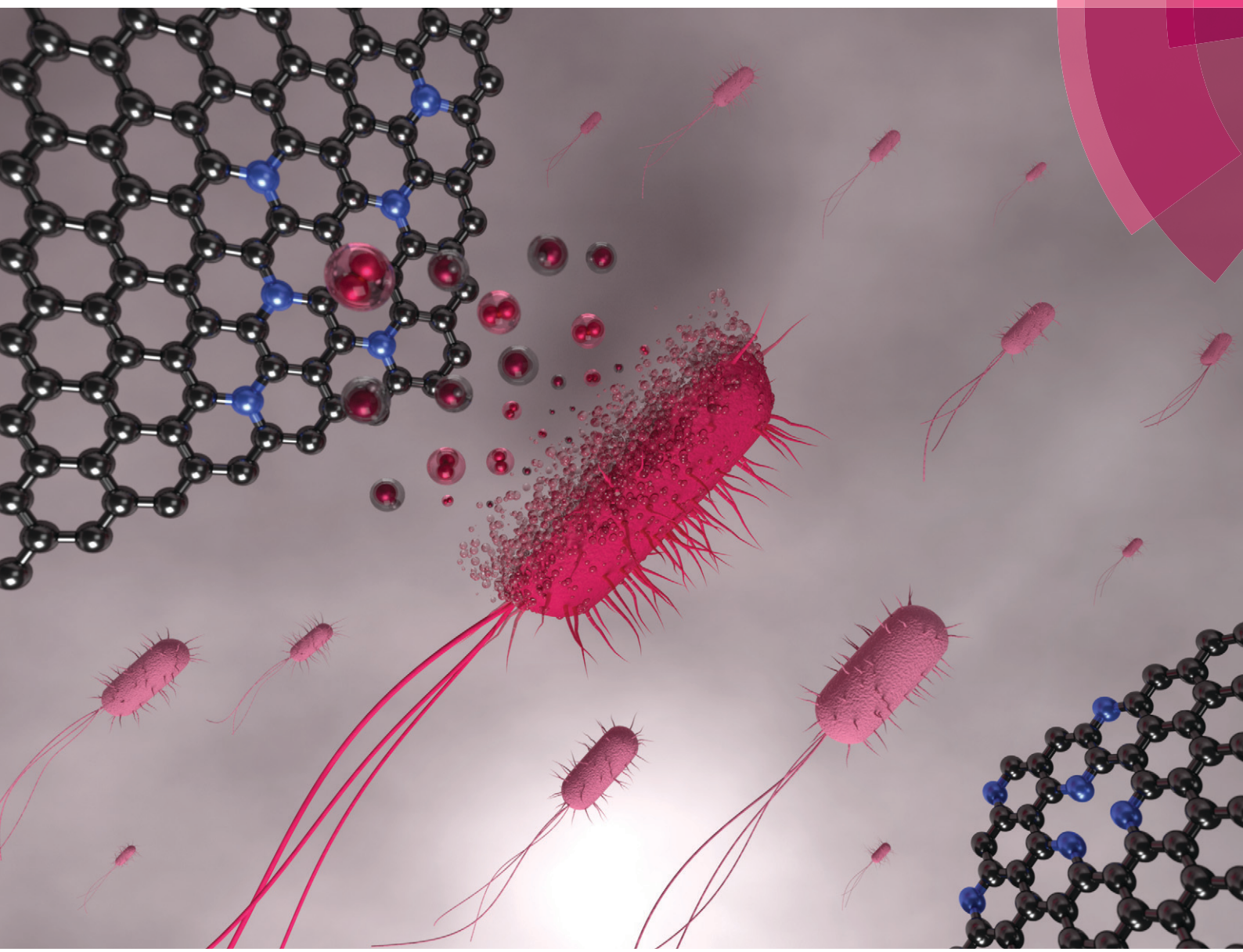

ISSN 2051-8153

ROYAL SOCIETY OF CHEMISTRY | Celebrating IYPT 2019

PAPER
Leanne M. Gilbertson *et al.*
Leveraging electrochemistry to uncover the role of nitrogen in the biological reactivity of nitrogen-doped graphene

Environmental Science Nano

PAPER

Cite this: *Environ. Sci.: Nano*, 2019, **6**, 3525

Leveraging electrochemistry to uncover the role of nitrogen in the biological reactivity of nitrogen-doped graphene†

Yan Wang, [a] Nathalia Aquino de Carvalho, [a] Susheng Tan [b] and Leanne M. Gilbertson *[ac]

Received 15th July 2019,
Accepted 6th September 2019

DOI: 10.1039/c9en00802k

rsc.li/es-nano

While nitrogen doping greatly broadens graphene applications, relatively little is known about the influence of this heteroatom on the biological activity of graphene. A set of systematically modified nitrogen-doped graphene (NG) materials was synthesized using the hydrothermal method in which the degree of N-doping and N-bonding type is manipulated using two nitrogen precursors (urea and uric acid) and different thermal annealing temperatures. The bioactivity of the NG samples was evaluated using the oxidation of the intracellular antioxidant glutathione (GSH) and bacterial viability (of *Escherichia coli* K12), and oxidative stress was identified as the predominant antibacterial mechanism. Two key energy-relevant electrochemical reactions, oxygen reduction reaction (ORR) and oxygen evolution reaction (OER), were used to characterize the influence of different N-types on the electronic properties of the NG materials. Electron-donating graphitic-N and electron-withdrawing pyridinic-N were identified as effective promoters for ORR and OER, respectively. The similar mechanisms between the GSH oxidation (indicative of oxidative stress) and ORR mechanisms reveal the role of graphitic-N as the active site in oxidative stress related bioactivity, independent of other consequential properties (*e.g.*, defect density, surface area). This work advances a growing rational design paradigm for graphene family materials using chemical composition and further provides valuable insight into the performance-hazard tradeoffs of NG applications in related fields.

Environmental significance

The ability to safely realize wide-ranging applications of graphene is limited by the inability to link properties that govern performance and that govern adverse impacts. Filling this gap will enable control of desired functional performance outcomes and adverse biological impacts through manipulations of graphene. Building on an established body of knowledge in graphene electrochemistry, the introduction of different N-bonding motifs is used to manipulate the electronic and bioactivity of N-doped graphene (NG). Key findings include, (i) similar trends between NG-mediated antioxidant oxidation and bacterial cytotoxicity suggesting a dominant oxidative stress mechanism and (ii) the correlation between the electrochemical oxygen reduction reaction and oxidative stress-related bioactivity demonstrating the important role of electron-donating graphitic-N in mediating bioactivity.

[a] *Department of Civil and Environmental Engineering, University of Pittsburgh, Pittsburgh, Pennsylvania 15261, USA. E-mail: leanne.gilbertson@pitt.edu; Tel: +(412) 624 1683*

[b] *Department of Electrical and Computer Engineering, Swanson School of Engineering and Petersen Institute of Nanoscience and Engineering, University of Pittsburgh, Pittsburgh, Pennsylvania 15261, USA*

[c] *Department of Chemical and Petroleum Engineering, University of Pittsburgh, Pittsburgh, Pennsylvania 15261, USA*

† Electronic supplementary information (ESI) available: Including the methodological details of material characterization techniques; the deconvoluted XPS N1s spectra to determine the distribution of N-types (Fig. S1); the Raman spectra including D, G peaks and 2D region (Fig. S2); the STEM-EDS elemental maps showing the distribution of C and O on the graphene (Fig. S3); the plots of ln [GSH] *versus* time to calculate the kinetic rates of GSH oxidation (Fig. S4); the electron transfer number *n* and the yield of H_2O_2 determined by RRDE (Fig. S5); the nitrogen adsorption–desorption isotherms to investigate the BET surface area (Fig. S6); and the photographs comparing the dispersion behavior of urea and uric acid samples (Fig. S7). See DOI: 10.1039/c9en00802k

Introduction

One-atom-thick and high-aspect-ratio graphene gives rise to advantageous electronic, thermal, optical, and mechanical properties that enable diverse applications in energy storage and conversion, electronics, and biotechnology.[1–6] Research on biological interactions of graphene-based nanomaterials and the ability to manipulate properties to influence interactions at bio-interfaces are critical for not only understanding potential risks that graphene poses to environmental and human health through increased use, but also for enabling their biomedical and bioanalytical development.[7–10] In addition, resolving the material properties that govern impacts of graphene-based nanomaterials at bio-interfaces is critical to developing rational design guidelines to meet desired

functional performance outcomes in these applications while minimizing the potential for unintended consequences.[11]

Chemical doping of graphene with heteroatoms, particularly nitrogen, is an effective approach to tailor electronic properties and chemical reactivity of graphene, which contributed to the emergence of (bio)electronic, (bio)sensor, electrocatalyst, and energy storage and conversion applications.[12–17] However, to date, very little is known about the influence of nitrogen doping on the biological activity of graphene. The similarity in the atomic size of nitrogen and carbon, and the five available valance electrons enable relatively facile replacement of carbon with nitrogen in the graphene lattice by forming strong covalent bonds.[14] Differences in electronegativity and electron density introduce charge redistribution between nitrogen dopants and adjacent carbon atoms. The resulting changes in spin density and charge distribution of these carbon atoms bring about more active sites on the graphene, accelerating electron transfer and improving the (electro)catalytic activity of graphene.[12,13,18–20] While pure graphene is a zero-bandgap semimetal, nitrogen doping shifts the Fermi level and opens up the bandgap, enabling the transformation of graphene to a n- or p-type semiconductor depending on the particular nitrogen configurations.[16,21–23] Nitrogen doping is a facile doping process that effectively modulates the structure and physicochemical properties of graphene while maintaining high electrical conductivity.[24]

Our previous study on reduced graphene oxide (rGO) demonstrates the positive correlation between electrochemical activity and the propensity to induce biological oxidative stress.[7] Decoupling these activities (*e.g.*, by identifying another structural or property feature that correlates independently with biological oxidative stress) would elucidate opportunities to design graphene family materials with enhanced electrochemical performance while reducing the potential for adverse biological impacts. Previous findings of nitrogen-doped carbon nanomaterials (carbon nanotubes, graphene, carbon dots) suggest the potential opportunity to decouple the governing properties due to suggested biocompatibility.[25–32] On the other hand, in our efforts to probe underlying mechanisms of electrochemical and biological reactions of oxygen functionalized carbon nanomaterials,[7–9] we identified electron transfer properties common to both activities that are similarly tuned by different surface functional groups. In this work, we investigate the potential for nitrogen doping to (i) decouple function and biological reactivity of graphene, and (ii) establish the foundation for a new paradigm linking inherent electronic and biological activities of carbon nanomaterials.

N-Doped graphene (NG) contains four primary nitrogen configurations in the graphene lattice: pyridinic-N, pyrrolic-N, graphitic-N, and N-oxide.[13,20,33,34] The nitrogen bonding configurations, not the total nitrogen content, have been identified as the key factor for the performance of important electrochemical reactions (*e.g.*, oxygen reduction reaction (ORR) and oxygen evolution reaction (OER)), with pyridinic-N or/and graphitic-N configurations commonly considered as active catalytic sites.[12,13,35–38] To further resolve the role of N in the biological activity of NG and the potential to decouple from electrochemical activities, we systematically prepared a set of NG materials with varying degrees of N-doping and different N-types using a hydrothermal method. The degree of nitrogen doping and configurations of nitrogen in doped graphene are tailored by using two different nitrogen precursors (urea and uric acid) and thermal annealing under different temperatures. The bioactivity of the prepared materials is evaluated as the inactivation of a bacterial model organism, *Escherichia coli* (*E. coli*) K12, and the propensity to oxidize an intracellular antioxidant, glutathione (GSH). Two important and well-studied electrochemical reactions, ORR and OER, are used (i) as representative functional performance metrics (relevant to energy-related electrochemical reactions), and (ii) to characterize the inherent electronic behavior of different NG materials as the potential mechanism underlying different biological activities.

Materials and methods

Chemicals and materials

Single layer graphene oxide (GO) powder (~99% purity) prepared using Hummer's method was purchased from ACS Materials LLC (Medford, MA, USA, product no. GNOP20A5), and used as the starting material to synthesize N-doped graphene. Uric acid (≥99%), methylene blue, platinum (20% on carbon black), iridium(IV) oxide (IrO_2, 99.99% metals basis), and Nafion perfluorinated resin solution (5 wt% in mixture of lower aliphatic alcohols and water) were obtained from Sigma-Aldrich (St. Louis, MO, USA). Urea (≥99%), reduced glutathione (GSH), bicarbonate ($NaHCO_3$), tris(hydroxymethyl)-aminomethane (TRIS, 99.85%), hydrochloric acid (HCl, 36.5–38%), Ellman's reagent (5,5′-dithio-bis-(2-nitrobenzoic acid), DTNB), dimethyl sulfoxide (DMSO, ≥99.9%), potassium hydroxide (KOH, 85.8%), isopropanol (molecular biology grade, ≥99.9%), sodium chloride (NaCl, 99.6%), Bacto agar, and Luria–Bertani (LB) Lennox broth (Lot 163 854) were obtained from Fisher Scientific (Pittsburgh, PA, USA). Polypyrrole was purchased from Toronto Research Chemicals (Toronto, ON, Canada). Deionized (DI) water was produced by Millipore Synergy UV Water Purification System and used as solvent for all chemicals, unless otherwise specified.

Synthesis of a systematic N-doped graphene material set

300 mg of GO was dispersed in 200 mL of deionized water by bath sonication (VWR Aquasonic 150T) for 1 h, and then mixed with urea in a 1 : 30 mass ratio and with uric acid in a 1 : 10 mass ratio, respectively. The mixture was stirred for 1 h and then sealed in a 300 mL Teflon-lined autoclave and remained at 175 °C for 12 h. After the autoclave was cooled down to the room temperature, the solids were filtered and washed and finally dried by lyophilization. The samples after this one-pot hydrothermal process are named as NG-U and NG-UA (*i.e.*, N-doped reduced GO (NG) with urea and uric

acid as the nitrogen precursor), respectively. One rGO sample was also prepared using the same experimental procedure but without addition of the N precursor, which serves as the control for NG-U and NG-UA samples.

Further, two annealed samples were prepared for each N-precursor set. NG-U or NG-UA was transferred to a tube furnace (Thermo Scientific Lindberg/Blue M TF55035A-1) and heated to the target temperature at a heating rate of 5 °C min^{-1} and annealed for 30 min under a helium gas flow. The samples after annealing NG-U at 650 °C and 950 °C are denoted by NG-U-650 and NG-U-950, respectively. The samples after annealing NG-UA at 650 °C and 800 °C are denoted by NG-UA-650 and NG-UA-800, respectively.

Material characterization

N-Doped graphene samples were characterized using X-ray photoelectron spectroscopy (XPS, to determine the elemental composition and distribution of N-types through peak deconvolution of N1s spectra), Raman spectroscopy (to determine defect density and the shift between n- and p-doping), transmission electron microscopy (TEM, to evaluate the morphology and obtain the mapping of elemental distribution), Brunauer–Emmett–Teller (BET) analysis (to measure the surface area), and methylene blue adsorption (to evaluate the dispersed surface area in suspension). The methodological details of these characterization techniques are described in the ESI.†

Evaluation of biological activity

GSH oxidation by the NG samples. GSH oxidation by the NG samples was evaluated following the same procedure detailed in our previous publications.[7–9,39] Briefly, reduced GSH (0.4 mM) was exposed to the NG samples (0.05 mg mL^{-1}, buffered at pH = 8.6) and monitored for 6 h in the dark at room temperature under constant rotation. Measurements were performed at different time points (0.25, 0.5, 1, 2.5, 4, and 6 h). At each time point, the suspension was passed through a 0.22 μm syringe filter (MilliporeSigma) to remove the graphene sample. 0.9 mL of the filtrate was then combined with 1.57 mL Tris-HCl buffer (pH = 8.3) and 30 μL of Ellman's reagent (0.1 M). The absorbance at 412 nm was measured using a UV-vis spectrophotometer and then used to determine the concentration of non-oxidized GSH. The percent loss of GSH was calculated compared to the control (no NG). Average and standard deviations were determined from three replicates.

Kinetic rates of GSH oxidation were calculated following our previous studies.[7,39] Rapid adsorption of reactant (*i.e.*, GSH) and desorption of product (*e.g.* glutathione disulfide) from the sample surface is assumed in the kinetic model. The interaction between GSH and the NG samples is expressed with the following first-order rate law:

$$-\frac{(\mathrm{d}[\mathrm{GSH}])}{\mathrm{d}t} = k[\mathrm{GSH}][\mathrm{NG}] \rightarrow \ln[\mathrm{GSH}] = -k[\mathrm{NG}]t + C \quad (1)$$

where k is the rate constant (mL mg^{-1} h^{-1}), [GSH] is the concentration of free GSH in solution, [NG] is the concentration of the NG sample (0.05 mg mL^{-1}), C is a constant of this integration equation and denotes the natural logarithm of the initial GSH concentration.

Antibacterial activity of the NG samples in suspension. E. coli K12 (CGSC #7740, Yale Coli Genetic Stock Center, New Haven, CT, USA) was used as a model Gram-negative bacterium to evaluate antimicrobial activities of the NG samples. Cultures were grown overnight in LB Lennox broth at 37 °C and harvested at mid-exponential phase. To remove residual growth-medium constituents prior to exposure to the prepared NG samples, cell cultures were (i) centrifuged at 10 000 rpm for 1 min to pellet cells, (ii) the supernatant was decanted and replaced with saline solution (0.9% NaCl), and (iii) the cells were re-suspended in saline solution. This washing step was repeated three times.

The NG samples (0.2 mg mL^{-1}) dispersed in saline solution were bath sonicated for 1 h before being exposed to the bacteria. For the exposure, 3 mL of the sonicated NG sample was mixed with 30 μL of bacteria solution (~10^7 colony forming units (CFU) mL^{-1}) for 4 h at room temperature under constant rotation. In addition to directly plating the suspension after 4 h exposure, the bacteria suspension was bath sonicated for 10 min after the 4 h reaction to release viable bacteria that are wrapped by NG aggregates, as in previous studies.[40–44] After both the exposure period and the sonication step, bacteria inactivation was evaluated using a colony counting method. Briefly, 100 μL of bacteria suspension was immediately plated on LB agar plates and incubated for 17 h at 37 °C for CFU enumeration. The percent inactivation was calculated by comparing the exposure to the control (*i.e.*, bacteria solution without the NG samples). All treatments were prepared in triplicate and repeated in three independent experiments. All materials and chemicals used for antimicrobial activity experiments were sterile.

GraphPad Prism version 8.1.0 (La Jolla, California, USA) was used to assess the difference in the GSH oxidation and the bacterial inactivation by rGO and NG samples. One-way ANOVA with Tukey's multiple comparison test was used to compare three or more treatments at each time point, and two-tailed *t*-test was used when there were only two treatments to compare. Moreover, linear regression model was applied for GSH oxidation results and the slopes of curves from different treatments were compared *via* the extra sum-of-squares F test. The significance level is 95%, *i.e.*, P values smaller than 0.05 are considered statistically significant.

Electrochemical measurements

For electrochemical characterization, the working electrodes were prepared as follows: (i) 2 mg of sample was mixed with 600 μL deionized water, 390 μL isopropanol, and 10 μL of Nafion (5 wt%) followed by 15 min probe sonication (Branson S-450 digital ultrasonic homogenizer) and 2 h bath sonication to form a well-dispersed suspension, (ii) 10 μL of the dispersed mixture was carefully deposited on the glassy carbon disk electrode surface (0.1963 cm^2) and dried at room

temperature for 2 h. The working electrodes were then tested in a three-electrode cell with a platinum counter electrode and an Ag/AgCl reference electrode. The values of potential are referenced against Ag/AgCl unless otherwise specified. Also, commercial noble metal catalysts Pt/C and IrO_2 were used as reference materials for ORR and OER, respectively.

The ORR experiments by rotating ring-disk electrode (RRDE) voltammetry were carried out using the same procedures described in our previous research.[7] Briefly, 1 M KOH electrolyte solution was used for all ORR experiments. Prior to each measurement, the electrolyte was bubbled with N_2 for 30 min and the working electrode was cleaned by cyclic voltammetry for 25 cycles sweeping from 0.2 to −1 V. Next, the electrolyte was saturated with O_2 for 30 min before performing RRDE tests. RRDE voltammetry was conducted from 0.2 to −1 V at a scan rate of 5 mV s^{-1} with varying rotating speeds of 400, 625, 900, 1600, and 2500 rpm. The ring potential was held at 0.5 V. The electron transfer number (n) and the percentage of H_2O_2 released during ORR were determined using the following equations:

$$n = \frac{4I_D}{I_D + \frac{I_R}{N}} \quad (2)$$

and

$$\%H_2O_2 = 200\times\frac{\frac{I_R}{N}}{I_D + \frac{I_R}{N}}, \quad (3)$$

where I_D is the measured disk current (mA), I_R is the measured ring current (mA), and N is the H_2O_2 collection coefficient at the ring (25.6%, provided by PINE Research Instrument). The onset potentials of ORR polarization curves were determined from the intersection of the tangents between the baseline and the rising reduction current.

The OER experiments using rotating disk electrode (RDE) were performed in 1 M KOH electrolyte from 0 to 0.7 V with a scan rate of 5 mV s^{-1} and a rotating speed of 1600 rpm. The electrolyte was saturated with O_2 before the experiments and the O_2 flow was maintained over the electrolyte during the measurements to ensure the O_2/H_2O equilibrium.

Results and discussion

Preparation and characterization of systematically modified N-doped graphene (NG)

Changing nitrogen precursors and annealing temperatures effectively tunes the N-doping states. The hydrothermal method was used to synthesize NG samples because it is a facile and eco-friendly method compared to other complex, low-yield, and costly techniques such as chemical vapor deposition and nitrogen plasma process.[14,34,35,45,46] The hydrothermal method has also been shown to attain a higher level of nitrogen doping compared to other methods such as thermal annealing, electrothermal reaction, and arc-discharge.[13,14,46] In the hydrothermal process, supercritical water acts as an alternative green reducing agent to organic solvents. Nitrogen precursors are mixed with GO in a hydrothermal autoclave reactor, and nitrogen doping occurs concomitantly with the elimination of oxygen groups on the GO. Given that nitrogen precursors affect the nature of N-types in NG,[47] urea and uric acid were used as nitrogen sources to introduce distinct properties and further different performance of samples between two precursor NG sets. A comparison of two precursor NG sets is anticipated to identify the governing material properties leading to more conclusive results.

There are four primary nitrogen configurations observed in NG: pyridinic-N, pyrrolic-N, graphitic-N, and N-oxide (Fig. 1).[13,20,33,34] Pyridinic-N and pyrrolic-N are located on graphene edges, the pyridinic structure is sp^2 hybridized and bonded to two carbon atoms while the pyrrolic structure is sp^3 hybridized and incorporated into a five-membered ring. Graphitic valley and center nitrogen configurations refer to the sp^3 N atoms within the six-membered carbons. N-Oxide refers to the nitrogen bonded with two carbon atoms and one oxygen atom. These nitrogen bonding types play profoundly different roles in tuning the graphene electronic properties, providing a p-type doping (electron-deficient, higher tendency to withdraw electrons) by pyridinic- and pyrrolic-N and a n-type doping (electron-rich, higher tendency to donate electrons) by graphitic-N.[16,22,23] The type of nitrogen introduced into the carbon lattice of our samples was tailored using thermal annealing at different temperatures (650, 800, 950 °C) after the hydrothermal reaction, leveraging different thermal stabilities of the N-types: graphitic-N > pyridinic-N > pyrrolic-N.[14,48]

XPS was used to quantify the amount and distribution of N-types on our different samples (data compiled in Table 1). The results confirm that nitrogen was successfully doped to the graphene lattice and that a systematic distribution of the four nitrogen configurations was achieved. A 9.17% and 6.86% total nitrogen is introduced into the graphene sheets for NG-U and NG-UA, respectively. Upon annealing, the total nitrogen content decreases to 5.70% for NG-U-950 and 3.84% for NG-UA-800, suggesting the removal of thermally unstable N species at these higher temperatures. The annealing treatment enables a self-arrangement and temperature-favored competition among different N-types (see details below on

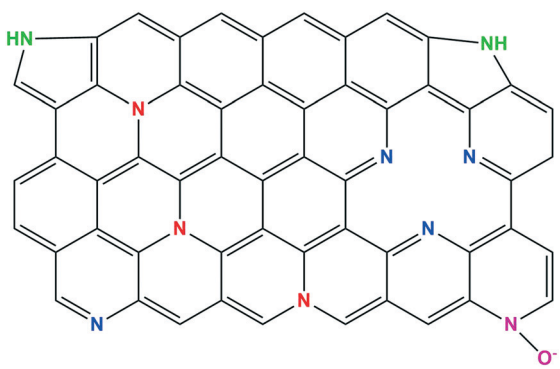

Fig. 1 Schematic N-doping configurations in N-doped graphene, including pyridinic-N (blue), pyrrolic-N (green), graphitic-N (red), and N-oxide (purple).

Table 1 Surface chemistry characterization data for N-doped graphene samples attained from XPS spectra, including the atomic percentage of C, O, and N. The atomic percentage of four predominant nitrogen configurations (pyridinic-N, pyrrolic-N, graphitic-N, and N-oxide) are identified from peak deconvolution of the N1s envelope. The values in the parentheses refer to the percentage distribution of four N-types

Samples	Annealing Temp. (°C)	% C	% O	% N	Pyridinic-N (% total N)	Pyrrolic-N (% total N)	Graphitic-N (% total N)	N-Oxide (% total N)
rGO	—	84.97 ± 0.46	15.03 ± 0.46	—	—	—	—	—
NG-U	—	82.26 ± 0.45	8.57 ± 0.08	9.17 ± 0.38	2.83 ± 0.06 (30.88%)	4.66 ± 0.11 (50.79%)	0.93 ± 0.01 (10.16%)	0.75 ± 0.04 (8.17%)
NG-U-650	650	88.10 ± 0.10	4.88 ± 0.06	7.01 ± 0.05	3.33 ± 0.04 (47.49%)	2.06 ± 0.04 (29.33%)	1.10 ± 0.01 (15.67%)	0.53 ± 0.01 (7.51%)
NG-U-950	900	90.58 ± 0.41	3.72 ± 0.35	5.70 ± 0.26	2.69 ± 0.08 (47.18%)	1.02 ± 0.07 (17.90%)	1.45 ± 0.02 (25.45%)	0.54 ± 0.05 (9.46%)
NG-UA	—	81.12 ± 0.83	12.02 ± 0.35	6.86 ± 0.48	1.01 ± 0.05 (14.73%)	4.97 ± 0.06 (72.50%)	0.65 ± 0.01 (9.47%)	0.23 ± 0.03 (3.29%)
NG-UA-650	650	91.13 ± 0.42	4.63 ± 0.44	4.24 ± 0.05	2.18 ± 0.03 (51.50%)	1.04 ± 0.03 (24.59%)	0.68 ± 0.04 (15.93%)	0.34 ± 0.02 (7.97%)
NG-UA-800	800	92.98 ± 0.23	3.18 ± 0.15	3.84 ± 0.15	1.96 ± 0.06 (51.10%)	0.54 ± 0.06 (14.11%)	0.97 ± 0.07 (25.20%)	0.37 ± 0.03 (9.58%)

(rGO = the reduced GO after one-step hydrothermal reduction without the addition of nitrogen precursors, serving as the control for NG-U and NG-UA samples; NG-U = N-doped rGO after one-step hydrothermal reduction with urea as the N precursor; NG-UA = N-doped rGO after one-step hydrothermal reduction with uric acid as the N precursor; NG-U-##0 or NG-UA-##0 = thermally annealed NG-U or NG-UA with the maximum temperature indicated by ##0)

the conversion between N-types). In addition, lower percent oxygen (O%) is observed for NG-U and NG-UA than for the rGO sample, suggesting that the N-doping process reduces oxygen functional groups on GO as a result of competitive doping between oxygen and nitrogen precursors.[38]

To quantify the relative amount of each N-type, the N1s spectra of NG samples were deconvoluted into four components (Fig. S1†). The binding energies for three main peaks including pyridinic-N, pyrrolic-N, and graphitic-N were assigned by constraining the peak positions to 398.7 eV (determined using a standard poly(3,5 pyridine)), 399.8 eV (determined using a standard polypyrrole), and 401.7 eV[49] (based on a previous study on a nearly pure graphitic-N doped graphene), respectively. The remaining small region centered at 404 eV was assigned to N-oxide, which is in good agreement with the literature.[15,33,34,36,50] The N-bonding configurations in the NG samples fabricated by the one-step hydrothermal method with either urea or uric acid (NG-U and NG-UA) are composed mainly of pyrrolic-N. The subsequent thermal treatment shifts the predominant N to pyridinic-N, for all samples. A decrease in percent pyrrolic-N and pyridinic-N and an increase in graphitic-N is observed after a further increase in the annealing temperature. These shifts occur due to different thermal stabilities of N-types, with graphitic-N being the most stable.[14,48] This conversion from pyrrolic-N to pyridinic-N or graphitic-N shifts the material propensity toward both electrochemical and biological activities.

Raman spectra reveal the changes in defect density and the shift between n- and p-type doping. Raman spectroscopy is used to characterize the changes in defect density by comparing the intensity ratio of the D and G peaks (I_D/I_G). It can also be used to differentiate the doping types (n- or p-type) based on the shift of G peak position (Fig. 2).[23,51,52] The broad bump-like 2D region (2400–3250 cm^{-1}) is observed for all samples (Fig. S2†), which is indicative of the high defect density regime.[7,53,54] In this regime, an increase of I_D/I_G indicates a decrease in defect density as opposed to the low defect density regime where the increase of I_D/I_G corresponds to an increase in defect density.[7,53,54] A higher I_D/I_G is noted for all NG samples compared to rGO, suggesting that N-doping reduces the defects by removing oxygen groups restoring the conjugated graphene structure. NG-U has the highest defect level (*i.e.*, lowest I_D/I_G ratio) among all doped samples. The annealing process after one-step hydrothermal process decreases the defect level through the reduction of N and O functionalities. The annealing at higher temperature does not significantly change the content of defects between NG-U-650 and NG-U-950, while NG-UA-800 exhibits a lower defect level than NG-UA-650.

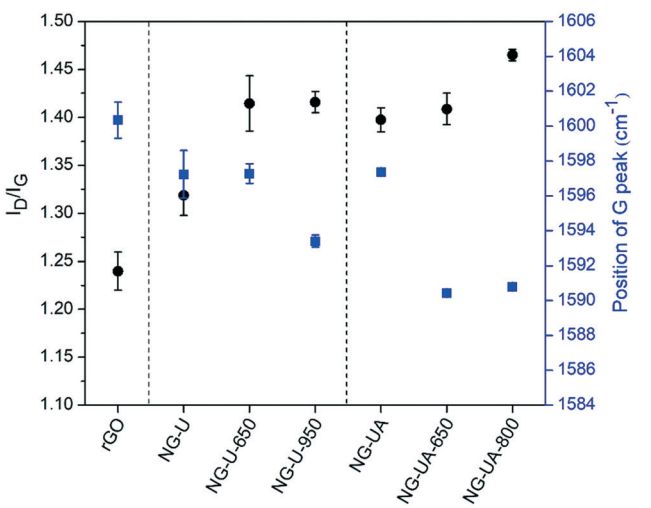

Fig. 2 Comparison of the I_D/I_G ratios (black circles, left *y*-axis) and the position of G peak (blue squares, right *y*-axis) for rGO and NG samples. The error bars stand for the standard deviation of triplicate measurements in different locations of each sample.

The effects of doping and the resultant compressive and tensile strain in graphene are possible origins for the shift of Raman peaks.[52] The shift of G peak position is a fingerprint of the concentration of charge carriers and dopants.[52] The downshift of G peak position could be attributed to the incorporation of N atoms leading to n-type doping (graphitic-N) while an upshift is observed for p-type doping (pyridinic-N, pyrrolic-N).[16,55] An upshift in the G peak at 1600 cm^{-1} is observed for the rGO sample compared to the value (~1580 cm^{-1}) reported for pure graphene without significant defects (*i.e.*, no D peak is observed).[51] This is due to the presence of residual oxygen functional groups causing a p-doping effect.[50] Upon being doped with N, the downshift of G peak position in NG-U and NG-UA suggests that the incorporation of N atoms reduces the effects of p-doping. A further downshift of G peak position is noted for the annealed samples, indicating an overall enhanced n-doping resulting from a higher content of graphitic-N, which agrees with XPS results.

No notable changes in graphene morphology are observed upon N-doping. TEM images of synthesized samples (Fig. 3), including undoped graphene (rGO), N-doped graphene (NG-U and NG-UA), and N-doped graphene with a further thermal treatment (NG-U-950 and NG-UA-800), show randomly compact and wrinkled multilayer graphene nanosheets. The structure of graphene morphology is well maintained after N-doping, and there is no apparent morphological difference among the five samples, suggesting that N-doping with different nitrogen precursors by the hydrothermal method and the subsequent thermal treatment do not influence the graphene morphology. The distribution of elements in the NG samples is shown by chemical mapping using STEM-EDS. A uniform distribution of N is shown in Fig. 3f–i, and that of C and O in Fig. S3.†

Identifying oxidative stress as the dominant mechanism of biological activity

The predominant mechanisms that are proposed to contribute to adverse biological impacts of graphene-based nanomaterials include chemical and physical pathways. Chemical mechanisms primarily refer to oxidative-stress induced by the graphene material, including direct redox reaction at bio-

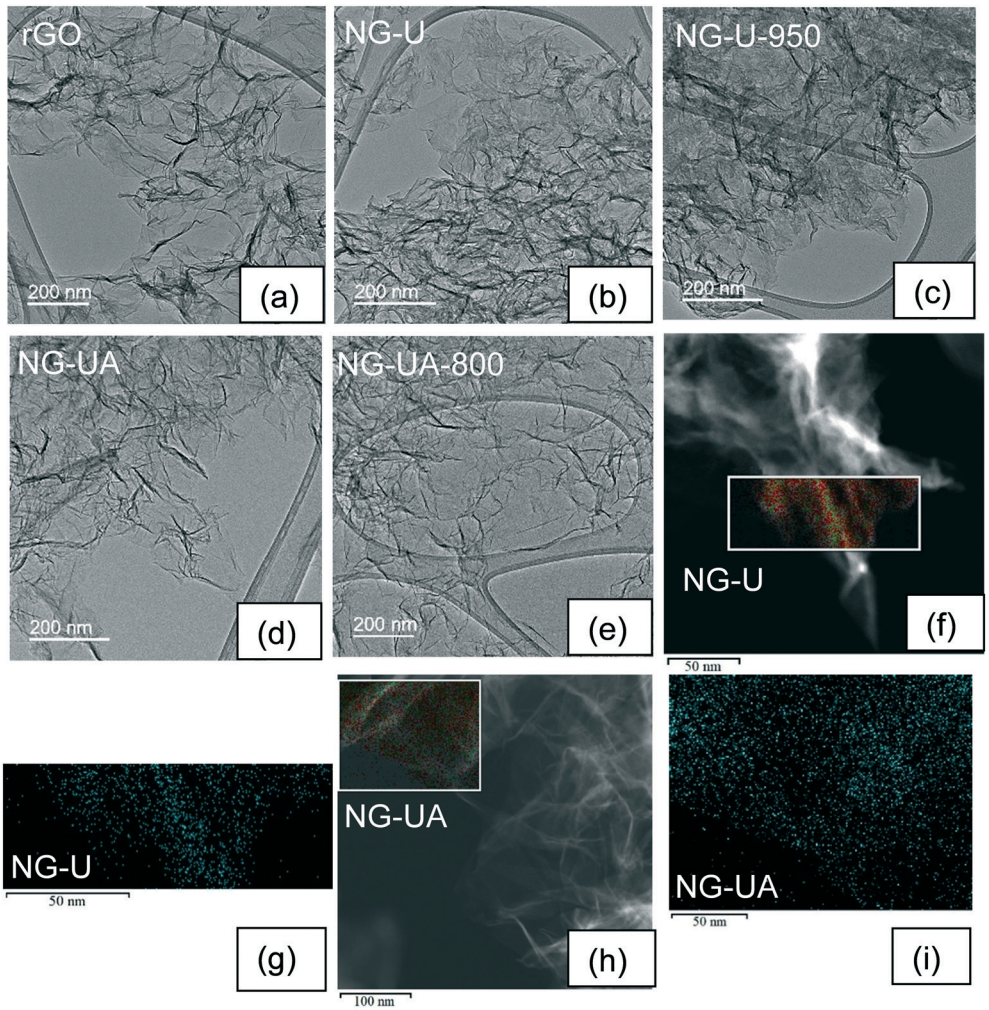

Fig. 3 TEM images of rGO (a), NG-U (b), NG-U-950 (c), NG-UA (d), NG-UA-800 (e), and STEM-EDS elemental maps of selected areas (f and h; red dots for C, green dots for O, and cyan dots for N) indicating the distribution of N (g and i, cyan dots) in NG-U and NG-UA, respectively.

interfaces or indirect *via* the production of reaction oxygen species (ROS).[40,56–59] Physical mechanisms include membrane-disruption imposed by the physical interaction with the graphene edges[56,59–61] and the wrapping or trapping of organisms given the unique thin 2D structure of graphene sheets.[40–43,59] The relative contribution of each mechanism and the ability to manipulate their magnitude of impact remain unresolved. Herein, different NG samples were found to exhibit different propensities for GSH oxidation and *E. coli* K12 inactivation, with the oxidative stress identified to be the dominant mechanism.

The oxidative potential of the NG sample set was assessed by the acellular oxidation of GSH. GSH is a cellular antioxidant and plays a major role in maintenance of a healthy redox balance[58,62] by oxidizing to its disulfide form (glutathione disulfide, GSSG)[62] to protect against exogenous oxidative agents, such as ROS.[63,64] The balance of GSH and GSSG serves as a predictor of the ability to defend oxidative stress.[65] Due to the close relevance of GSH to oxidative stress, GSH oxidation is commonly used to probe the level of oxidative stress imparted by graphene-based nanomaterials.[7,40,56,58] Further, given that oxidative stress has been shown to be a major mechanism for bacterial cytotoxicity of graphene-based nanomaterials,[41,56] the depletion of GSH can be correlated with antibacterial activity wherein the effects of bacterial inactivation result from the chemical pathway (*i.e.*, by oxidative stress).

GSH was exposed to rGO and NG samples for 6 h and the measurement of the non-oxidized portion of GSH was conducted using Ellman's assay at 1, 2.5, 4, and 6 h. Due to the high activity of NG-UA-650 and -800, additional data was collected at 0.25 and 0.5 h. The magnitude of GSH oxidation is different for the differentially treated samples (Fig. 4a), while the relative trend between the samples is maintained at all measured timepoints. The kinetic rate constants (k, mL mg^{-1} h^{-1}) determined from the slope of the linear curve fits (ln[GSH] *versus* time, Fig. S4†) follow the order: NG-U-650 (2.30) < rGO (2.84) < NG-U-950 (7.33) < NG-U (7.97) < NG-UA (13.14) < NG-UA-650 (94.40) < NG-UA-800 (208.27), with a strong fit to the first-order kinetic model ($R^2 > 0.98$). The effect of nitrogen precursors (urea and uric acid) on the oxidative capacity of samples toward GSH is significant; the samples with uric acid as the N-precursor (NG-UA, NG-UA-650 and -800) oxidize GSH considerably faster than those prepared from urea (NG-U, NG-U-650 and -950). Annealing temperatures are also found to influence the oxidative potential of NG samples. As the annealing temperature increases from 650 °C to 800 °C (for uric acid samples) and from 650 °C to 950 °C (for urea samples), GSH oxidation increases from 83% to 100% at 0.5 h and from 46% to 88% at 6 h for samples synthesized from uric acid and urea, respectively. Interestingly, while the annealed samples within the uric acid sample set (NG-UA-650 and -800) induce a higher GSH loss than the non-annealed sample (NG-UA), this trend does not hold for urea samples. NG-U causes similar GSH oxidation compared to NG-U-950, both of which are significantly higher than NG-U-650. The combined GSH oxidation results demonstrate that the prepared samples, with different C : N compositions and distributions of N-types, have different oxidative potentials suggesting induction of differential magnitudes of oxidative stress to bacterial cells.

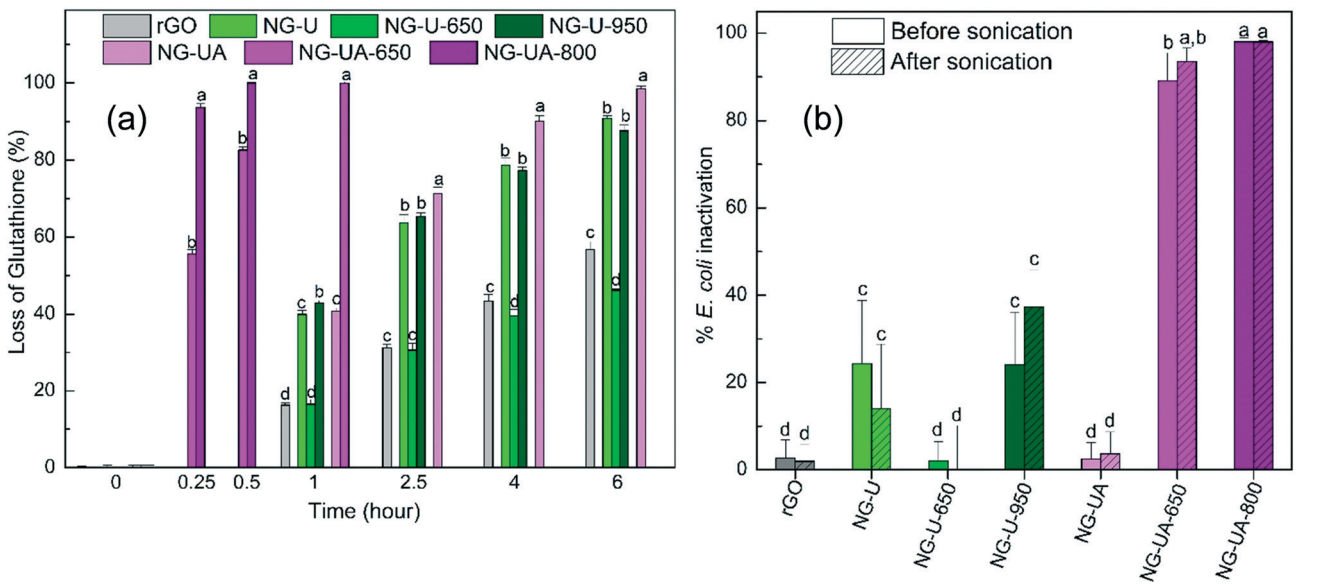

Fig. 4 (a) Glutathione (GSH) oxidation by rGO and NG samples for a total 6 h of incubation compared to the control (no rGO/NG). The mass loading of samples is 0.05 mg mL^{-1} and the initial concentration of GSH is 0.4 mM. (b) Cytotoxicity of rGO and NG samples to *E. coli* K12 after 4 h of reaction to 0.2 mg mL^{-1} sample before and after 10 min bath sonication to release viable bacteria wrapped in aggerated graphene sheets. The data were normalized to the control (saline solution without rGO/NG), the cell concentration of the control remained constant after the 4 h incubation and after the 10 min sonication. Means suffixed with different letters (a–d) for each time point are significantly different from each other at $P < 0.05$. Error bars denote the standard deviations of sample replicates.

The antibacterial activity of the NG sample set to the model bacterium *E. coli* K12 was evaluated. A similar trend is observed among the samples for *E. coli* K12 inactivation (Fig. 4b) and GSH oxidation (Fig. 4a). For example, increasing the annealing temperature leads to a higher magnitude of cytotoxicity (NG-U-950 > NG-U-650 and NG-UA-800 > NG-UA-650) and the two annealed uric acid samples (NG-UA-650 and -800) demonstrate the highest GSH oxidation and highest bacterial inactivation. The similar trends suggest that while physical proximity of the graphene material to the bacteria cell is necessary to induce a response, the dominant mechanism of cytotoxicity is chemical in nature rather than physical puncturing (see additional explanation below). The hydrothermal and thermal annealing treatments do not significantly affect the structure and morphology of the prepared NG samples (see Fig. 3), suggesting that the physical disruption mechanism induced by sharp edges of graphene (if it exists) is not likely explanations for the observed differences in bacterial cytotoxicity. Rather, the difference in the observed cytotoxic potentials among our samples (*e.g.*, $a > 90\%$ loss of cell viability for NG-UA-650 and -800 *versus* $a < 5\%$ of that for rGO, NG-U-650, and NG-UA) indicates that cell damage is induced through oxidative stress mechanisms rather than physical disruption.

The potential influence of a physical wrapping mechanism has been proposed and can confound conventional culturing approaches to evaluating cytotoxicity by inhibiting bacterial proliferation on agar plates. The effect of wrapping is typically investigated by releasing trapped cells through a mild bath sonication prior to plating.[40–44] In agreement with previous studies,[41,42,44] cell entrapment by the NG samples is not observed as there is no statistically significant decrease ($P > 0.05$) in cell viability loss before and after sonication (Fig. 4b). The combined results from the GSH oxidation and the cell inactivation support the dominant role of oxidative stress in the biological reactivity of our NG samples and their diverse oxidative potential.

Evaluation of oxygen reduction reaction (ORR) and oxygen evolution reaction (OER) validates different electron transfer properties as a function of N-type

ORR and OER are electrochemical processes that underlie clean energy technologies, including water splitting, fuel cells, and metal–air batteries.[6,13,17] Graphene-based nanomaterials have been pursued as metal-free catalysts to replace the noble-metal commercial catalysts (*e.g.*, Pt, Ir, Ru) that are scarce and high-cost.[6,12,13,17] Further, nitrogen-doped graphene has been extensively studied in the field of ORR and OER.[12,13,35–37] As such, ORR and OER are used in this work to represent the desired functional performance of NG materials. Also, given the importance of oxygen and electron transfer in the mechanisms of biological activities,[7–9] the evaluation of ORR and OER activities of NG will be useful for a better understanding of the underlying mechanism of interaction at the bio-interface. Herein, the evaluation of functional electrochemical activities, ORR and OER, of NG samples validates different electron transfer properties as a function of nitrogen type.

The enhanced ORR and OER activities are driven by properties of graphene-based materials, including the (i) electrical conductivity for electron transport within the graphene plane,[66–68] (ii) defects (topological and edge defects) that offer active sites,[69,70] (iii) electroactive surface area available for accessing active sites,[68] and (iv) presence of functionalities (*e.g.*, pyridinic-N, graphitic-N) that induce active sites for accelerating the adsorption of targets (and the intermediates) and favor electron transport for the reaction.[36,37,71] While the ORR reduces O_2 to H_2O, OER can be considered the opposite reaction in which H_2O oxidizes to O_2. Considering this inherently different mechanisms between ORR and OER, the active N moieties in NG to influence each activity will depend on their ability to donate or withdraw electrons.

ORR and OER are commonly carried out in a hydrodynamic condition. This enhances mass transfer by inducing convection so that steady-state diffusion is achieved, enabling elucidation of the kinetics and the mechanism of electrode reactions with high precision measurements.[72] RRDE and RDE measurements were performed for ORR and OER, respectively. Both experiments were conducted in alkaline media due to the advantages in terms of a decreased overpotential and a less corrosive environment compared to the process in acidic media.[73] Enhancement in ORR and OER activities is typically represented by a more positive onset potential and a higher absolute value of the current density on the potential–current polarization curves.

Trends in ORR polarization curves for rGO and NG samples are displayed in Fig. 5a with the Pt/C curve shown for comparison. While rGO and NG samples demonstrate a poor ORR activity compared to Pt/C (as the reference), different ORR activity is observed between samples, with the trend in onset potential: NG-U-650 (−0.189 V) < rGO (−0.179 V) < NG-UA (−0.169 V) ~ NG-UA-650 (−0.169 V) < NG-U-950 (−0.164 V) < NG-U (−0.159 V) < NG-UA-800 (−0.149 V). After the one-step hydrothermal synthesis, NG-U demonstrates a better electrochemical activity than NG-UA, indicating there are different interactions between urea and uric acid with GO during the hydrothermal synthesis. The subsequent annealing process results in a more pronounced increase in the electrochemical reactivity of samples within the uric acid precursor set than that within the urea precursor set.

The electron transfer number (n) and the H_2O_2 yield (H_2O_2%) were calculated by employing RRDE (Fig. S5†). ORR in alkaline media can occur by either a two-electron ($O_2 + H_2O + 2e^- \rightarrow HO_2^- + OH^-$, $HO_2^- + H_2O + 2e^- \rightarrow 3OH^-$) or a four-electron ($O_2 + 2H_2O + 4e^- \rightarrow 4OH^-$) pathway thus, a higher n represents a lower H_2O_2 yield. The four-electron pathway is advantageous for energy applications because the H_2O_2 intermediates produced in the two-electron pathway will deteriorate the catalysts and lead to a decline in the O_2 utilization rate.[74] At the potential ranging from −0.4 to −1.0 V, the n calculated for all samples falls within a range of 3.5 (25% H_2O_2) to 3.9 (5% H_2O_2), suggesting a predominant

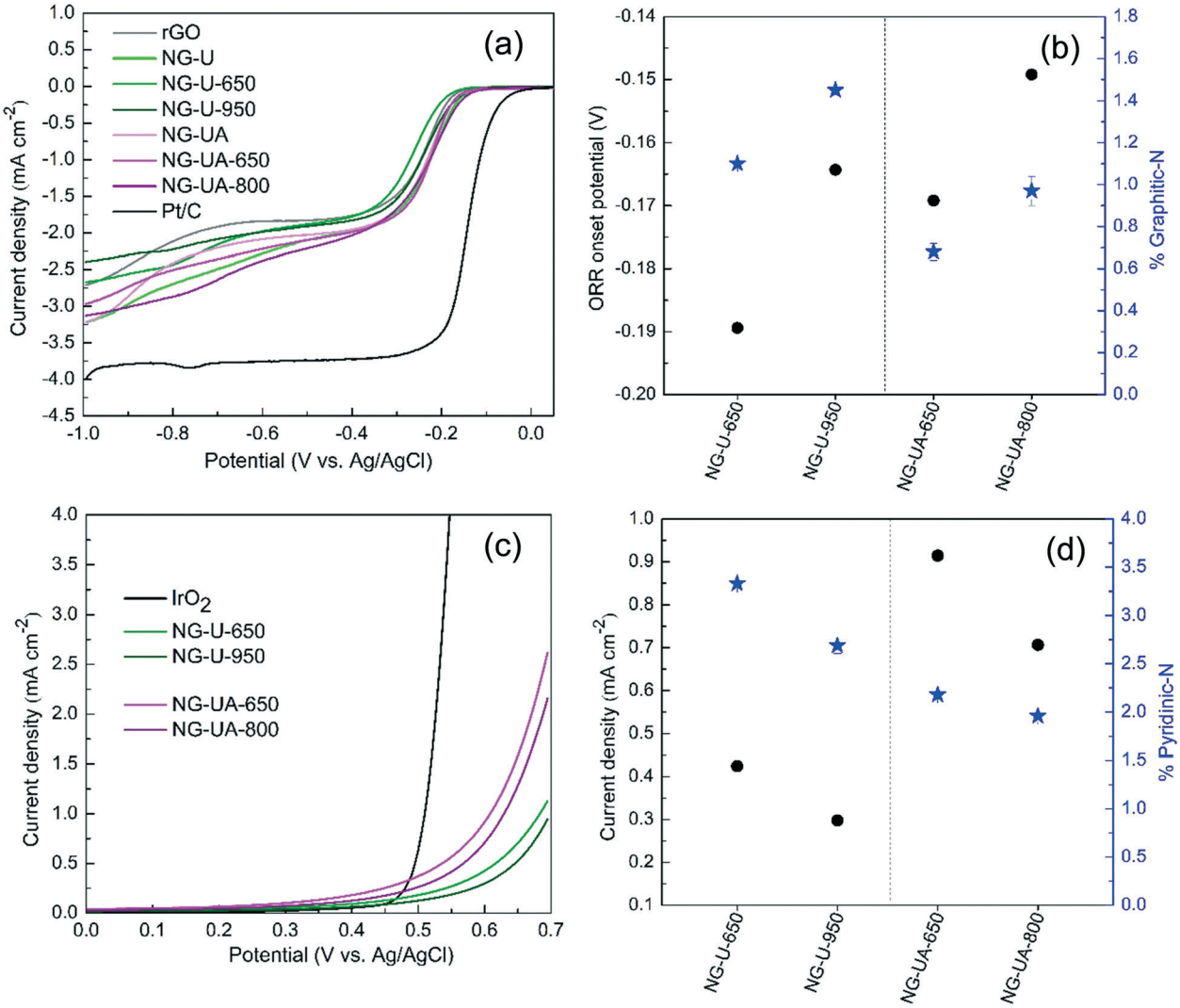

Fig. 5 (a) ORR polarization curves of rGO, NG samples, and Pt/C on RRDE in O_2 saturated 1 M KOH with a rotation rate of 1600 rpm and a scan rate of 5 mV s^{-1}. (b) The correlation between the ORR performance of NG (represented by the onset potential) and the percent of graphitic-N (determined by XPS). (c) OER polarization curves of annealed NG samples and IrO_2 on RDE in O_2 saturated 1 M KOH with a rotation rate of 1600 rpm and a scan rate of 5 mV s^{-1}. (d) The correlation between the OER performance of annealed NG samples (represented by the current density at a potential of 0.6 V) and the percent of pyridinic-N (determined by XPS).

4-electron oxygen reduction pathway. In general, NG-UA and NG-UA-650 show a lower n than rGO over this potential range while other samples enhance n, which suggests that the C : N compositions and distribution of N-types influence the reduction pathway.

The capacity of graphene materials to catalyze ORR depends on the defect density because defect sites can enhance the O_2 adsorption.[58] The higher defect density in NG-U explains the favorable reactivity toward ORR. While annealing decreases the defect density and subsequently suppresses the ORR activity, we observe an increasing ORR trend between NG-U-650 and NG-U-950 (having similar defect density), and between NG-UA-650 and NG-UA-800 (the latter having a lower defect density). This indicates that another property of these materials is involved in the observed difference in ORR activity. The proportion of different N-types, rather than the nitrogen content on the graphene, has been proposed to play an important role in the facilitation of electrocatalytic activity.[37,71,75,76] Graphitic-N possesses the electron-donating characteristic[16,22,23] and greater charge carrier transport over other N-types.[21,22] Graphitic-N atoms can lower the O_2 adsorption barrier by decreasing the repulsive interaction between graphene π electrons and lone pair electrons of O_2,[71,76] and can facilitate the donation of electrons to the adsorbed O_2 to form OOH species,[37,77] both of which are key steps to enhance the reduction of O_2 in alkaline solution. As a result, the samples annealed at higher temperatures demonstrate enhanced reactivity toward ORR due to the increase in the content of graphitic-N (Fig. 5b).

The electrocatalytic activity of the annealed samples within urea and uric acid precursor sets was investigated toward OER to determine whether the predicted opposing

trend is observed as predicted; samples with more pyridinic-N would have a greater propensity toward OER. Indeed, the opposite trend (Fig. 5c and d) is observed for OER compared to that for ORR. The samples annealed at higher temperatures (having 2.69% and 1.96% pyridinic-N for NG-U-950 and NG-UA-800, respectively) demonstrate lower OER activity in terms of the current density than that at lower temperatures (having 3.33% and 2.18% pyridinic-N for NG-U-650 and NG-UA-650). The carbon adjacent to electron-donating graphitic-N atoms possesses a partial negative charge (δ^-) and therefore can serve as nucleophiles. This behavior is unfavorable for the adsorption of intermediates necessary for water oxidation in the alkaline media (*e.g.*, OH^-, OOH^-).[37,75] Carbon atoms adjacent to electron-withdrawing pyridinic-N atoms carry a partial positive charge (δ^+), thus serving as electrophiles facilitating the adsorption of intermediates necessary for water oxidation (*e.g.*, OH^-, OOH^-).[37,78] In addition, the polarized pyridinic-N (δ^-) is not favorable for the reduction of O_2 due to its high density of N lone pair electrons that cause strong repulsive interaction with the O_2 approaching its adjacent carbon atoms.[71] Consequently, the samples annealed at higher temperatures demonstrate lower reactivity toward OER owing to the decrease in the pyridinic-N content.

While samples annealed with uric acid (NG-UA-650 and -800) contain lower percentage of graphitic-N and pyridinic-N than those within urea sample set (NG-U-650 and -950), the uric acid sample set presents an overall higher ORR and OER (Fig. 5b and d). This observation suggests another property in contributing to the sample activity and is attributed to the higher surface area of the uric acid materials (Fig. S6†). The BET surface area for NG-UA-800 is 549.3 $m^2\ g^{-1}$ and 428.2 $m^2\ g^{-1}$ for NG-U-950, enhancing access to the active sites that facilitate the electrocatalytic activities. The observed differences in BET surface area is maintained when the respective materials are dispersed (see additional details below).

Taken together, the characterization data indicate that multiple physicochemical properties of NG influence the electrochemical performance (here, ORR and OER activities). While the consequential material properties that result from N-doping (*e.g.*, defect density, surface area) influence ORR and OER synchronously, opposite trends observed for ORR and OER highlight the significant role of N-types in mediating these two electrochemical activities. While electron-donating graphitic-N and electron-withdrawing pyridinic-N are effective promoters for ORR and OER, respectively, the defect density and surface area that result from different preparation methods (precursors and annealing temperatures) further contribute to the material activity.

The similarity between glutathione (GSH) oxidation and oxygen reduction reaction (ORR) reveals the role of graphitic-N as the active site in oxidative stress related bioactivity

The evaluation of biological activity of our NG sample set highlights the essential role of oxidative stress at bio-interfaces and affirms that the oxidation of GSH is a good predictor of oxidative stress delivered by our NG samples. Previous studies propose that graphene family nanomaterials catalyze GSH oxidation through electron transfer with dissolved oxygen at the defect sites.[42,58] The dissolved oxygen (O_2) reacts with active defect sites on graphene forming surface-bound oxygen intermediates (*e.g.*, superoxide anion O_2^-, hydroperoxide OOH) that can oxidize GSH or be released to the bulk solution to form ROS that react with GSH.[58] The rate-limiting step for the oxidation of GSH is the formation of the surface oxide intermediates (O_2^-, OOH), similar to mechanism for ORR on the electrode surface in alkaline solution. Since O_2 has a high bond dissociation energy, it is not uniformly favorable and requires the formation of intermediates (O_2^-, OOH) that have lower bond dissociation energy.[73,75] As such, the oxidation of GSH and ORR share a similar mechanism, both of which are dominated by O_2-mediated catalytic process to reduce O_2 that starts with O_2 adsorption on the active sites of graphene materials.[58,73] It is thus expected that graphitic-N can influence the capacity of NG to oxidize GSH, as it does for ORR.

Similar trends are observed for the oxidation of GSH and the ORR activity within each N-precursor set (urea *versus* uric acid in Fig. 6a). As with the ORR trends described above, the important contribution of defects to the oxidization of GSH is underlined by the higher defect density in NG-U than the two annealed samples (NG-U-650 and -950, see Fig. 2). The samples annealed at higher temperatures within each N-precursor show an increased oxidative potential toward GSH, which is attributed to the increase in the percent of graphitic-N. Yet similar to the ORR trend described above, the samples prepared with the uric acid precursor have lower amounts of graphitic-N than those prepared with urea while exhibiting higher oxidative potential, which is believed to result from the increase in available surface area. Since the GSH assay is performed in the aqueous media, the dispersed surface area of the samples was evaluated by the adsorption of methylene blue (Fig. 6b). This approach is regarded as a standard method for measuring the surface area of graphitic materials in the aqueous phase.[45,79] Overall, a higher surface area corresponds with a better dispersion, which is observed for the uric acid samples. A visual comparison of their dispersion in water is shown in Fig. S7.† The increase in the thermal annealing temperatures induces a reduction in the dispersed surface area in both sample sets. This is caused by the removal of surface functionalities, which promotes aggregation of the samples in suspension, thus decreasing the available dispersed surface area.

Collectively, the data support multiple factors synergistically influencing the NG-mediated oxidation of GSH. In addition to the defect density and dispersed surface area, uncovering the role of graphitic-N in both ORR and GSH oxidation elucidates the underlying mechanisms of oxidative-stress induced biological activity. The similarities in ORR and GSH trends suggest the potential to employ electrochemical

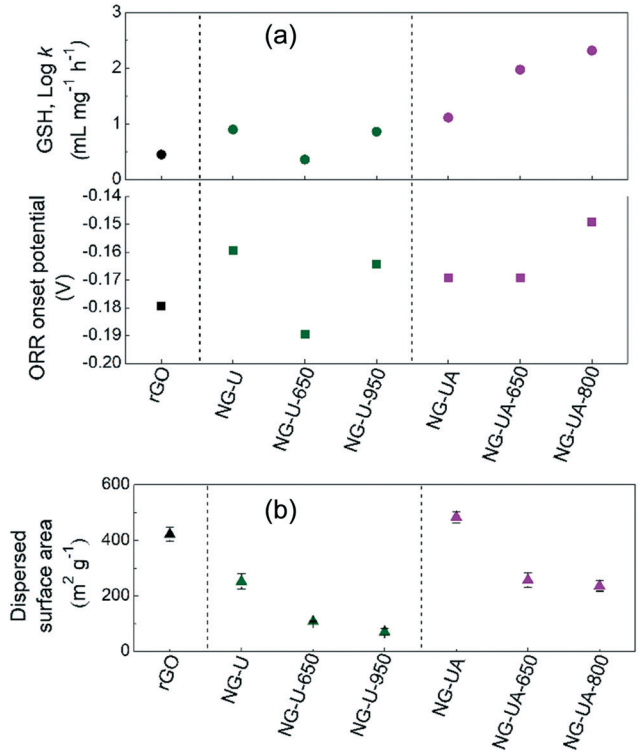

Fig. 6 (a) The correlated trends between the rate constants for GSH oxidation and the onset potentials for the ORR activity. (b) The dispersed surface areas in suspension determined by the adsorption of methylene blue.

tools to evaluate the relative bioactivity of graphene materials *via* chemical pathways.

The opportunity to tailor functional performance and inherent hazard outcomes

Sustainable design of nanomaterials defines a proactive approach to advance new applications while reducing the potential to introduce hazards to human health and the environment.[11,80] Results from this study demonstrate that governing N-types are distinct for electrochemical applications given their unique electronic properties. Specifically, graphitic-N is responsible for the reduction of oxygen (ORR) while pyridinic-N is responsible for water oxidation (OER). This suggests the ability to tune performance based on chemical composition, which we demonstrate is possible using different N-precursors and annealing temperatures. While the goal of a sustainable design approach is to enhance functional performance while reducing inherent bioactivity (GSH oxidation, cytotoxicity), a possible outcome is that the same material property modulates both outcomes. This was the result in our previous research on GO/rGO[7–9] as well as in this study for NG and ORR performance. Yet, in studying N-doped graphene herein, we discovered that the ability to decouple functional performance and bioactivity will depend on the desired performance outcome (*i.e.*, ORR *versus* OER). For example, the functional performance of OER is facilitated by pyridinic-N and the samples with high pyridinic-N have lower oxidative potential, thus suggesting a path toward enhanced performance without high bioactivity. While we used two approaches to modulate N-types of NG, there are many more options that enable further control of N doping to obtain closer to pure graphitic or pyridinic C–N bonding configuration[49,71] and advance the intended rational sustainable design for their applications.

Conclusions

The type of N that is incorporated in the graphene structure depends on how the sample is prepared, including the nature of N precursors and annealing temperatures. The different amount of doped N and the relative abundance of N-types differentially influence biological and electrochemical activities. Defect density and surface area are consequential properties that result from changes in N-content and work in concert with chemical composition to modulate both activities. While this work identifies these three properties to govern the measured outcomes (*i.e.*, GSH oxidation, bacterial inactivation, ORR, and OER), the contribution of each property to each outcome differs. For example, the trends in GSH oxidation and bacterial inactivation for the uric acid and urea sample sets are similar, yet the magnitude of the difference between individual samples differs for these two measured biological activities (Fig. 4a *versus* 4b). These findings elucidate the opportunity to tune (un)desired properties and material activities by modifying graphene chemistry.

While both electrochemical and biological activities are controlled by a balance between multiple properties, the type of N has an overarching effect. Electron-donating graphitic-N is responsible for ORR and O_2-mediated oxidative stress in bioactivity while electron-withdrawing pyridinic-N is responsible for enhancement in OER. Identification of N active sites for biological activities is useful to guide the development of N-doped graphene materials for their biomedical and bioanalytical applications. From the perspective of rational design, N-types can be leveraged as a design handle to tailor properties of graphene for specific applications while reducing or maintaining minimal adverse biological effects.

Finally, there is growing evidence of the correlation between electrochemical activity and biological reactivity of carbon nanomaterials including multi-walled carbon nanotubes,[8,9] graphene oxide,[7] and N-doped graphene (in the present work). Uncovering the underlying electronic nature of graphene, including the ability to engage in electron exchange and transport, is critical to informing the ability to rationally design graphene materials for electrochemical applications while also advancing predictive toxicity capabilities.

Conflicts of interest

There are no conflicts to declare.

Acknowledgements

The authors acknowledge generous financial support provided by the National Science Foundation CBET Award No. 1709031 and the University of Pittsburgh Central Research Development Fund. The authors thank Dr. Howard Fairbrother for his time, insight, and guidance provided for robust XPS deconvolution quantifying different N-types, and Dr. Yahui Yang for assistance with the BET surface area measurement.

References

1 A. McWilliams, *The Maturing Nanotechnology Market: Products and Applications*, BCC Research, NAN031G, 2016.
2 D. Jariwala, V. K. Sangwan, L. J. Lauhon, T. J. Marks and M. C. Hersam, Carbon Nanomaterials for Electronics, Optoelectronics, Photovoltaics, and Sensing, *Chem. Soc. Rev.*, 2013, **42**(7), 2824–2860.
3 J. Hou, Y. Shao, M. W. Ellis, R. B. Moore and B. Yi, Graphene-Based Electrochemical Energy Conversion and Storage: Fuel Cells, Supercapacitors and Lithium Ion Batteries, *Phys. Chem. Chem. Phys.*, 2011, **13**(34), 15384–15402.
4 H. Zheng, R. Ma, M. Gao, X. Tian, Y.-Q. Li, L. Zeng and R. Li, Antibacterial Applications of Graphene Oxides: Structure-Activity Relationships, Molecular Initiating Events and Biosafety, *Sci. Bull.*, 2017, **63**(2), 133–142.
5 G. Reina, J. M. González-Domínguez, A. Criado, E. Vázquez, A. Bianco and M. Prato, Promises, Facts and Challenges for Graphene in Biomedical Applications, *Chem. Soc. Rev.*, 2017, **46**(15), 4400–4416.
6 C. Hu and L. Dai, Carbon-Based Metal-Free Catalysts for Electrocatalysis beyond the ORR, *Angew. Chem., Int. Ed.*, 2016, **55**(39), 11736–11758.
7 Y. Wang and L. M. Gilbertson, Informing Rational Design of Graphene Oxide through Surface Chemistry Manipulations: Properties Governing Electrochemical and Biological Activities, *Green Chem.*, 2017, **19**(12), 2826–2838.
8 L. M. Pasquini, R. C. Sekol, A. D. Taylor, L. D. Pfefferle and J. B. Zimmerman, Realizing Comparable Oxidative and Cytotoxic Potential of Single-and Multiwalled Carbon Nanotubes through Annealing, *Environ. Sci. Technol.*, 2013, **47**(15), 8775–8783.
9 L. M. Gilbertson, D. G. Goodwin Jr., A. D. Taylor, L. Pfefferle and J. B. Zimmerman, Toward Tailored Functional Design of Multi-Walled Carbon Nanotubes (MWNTs): Electrochemical and Antimicrobial Activity Enhancement via Oxidation and Selective reduction, *Environ. Sci. Technol.*, 2014, **48**(10), 5938–5945.
10 Z. Wang, W. Zhu, Y. Qiu, X. Yi, A. von dem Bussche, A. Kane, H. Gao, K. Koski and R. Hurt, Biological and Environmental Interactions of Emerging Two-Dimensional Nanomaterials, *Chem. Soc. Rev.*, 2016, **45**(6), 1750–1780.
11 L. M. Gilbertson, J. B. Zimmerman, D. L. Plata, J. E. Hutchison and P. T. Anastas, Designing Nanomaterials to Maximize Performance and Minimize Undesirable Implications Guided by the Principles of Green Chemistry, *Chem. Soc. Rev.*, 2015, **44**(16), 5758–5777.
12 J. Zhang and L. Dai, Heteroatom-Doped Graphitic Carbon Catalysts for Efficient Electrocatalysis of Oxygen Reduction Reaction, *ACS Catal.*, 2015, **5**(12), 7244–7253.
13 J. Duan, S. Chen, M. Jaroniec and S. Z. Qiao, Heteroatom-Doped Graphene-Based Materials for Energy-Relevant Electrocatalytic Processes, *ACS Catal.*, 2015, **5**(9), 5207–5234.
14 X. Wang, G. Sun, P. Routh, D.-H. Kim, W. Huang and P. Chen, Heteroatom-Doped Graphene Materials: Syntheses, Properties and Applications, *Chem. Soc. Rev.*, 2014, **43**(20), 7067–7098.
15 H. Wang, T. Maiyalagan and X. Wang, Review on Recent Progress in Nitrogen-doped Graphene: Synthesis, Characterization, and Its Potential Applications, *ACS Catal.*, 2012, **2**(5), 781–794.
16 H. Liu, Y. Liu and D. Zhu, Chemical Doping of Graphene, *J. Mater. Chem.*, 2011, **21**(10), 3335–3345.
17 X. Liu and L. Dai, Carbon-Based Metal-Free Catalysts, *Nat. Rev. Mater.*, 2016, **1**(11), 16064.
18 L. Zhang and Z. Xia, Mechanisms of Oxygen Reduction Reaction on Nitrogen-Doped Graphene for Fuel Cells, *J. Phys. Chem. C*, 2011, **115**(22), 11170–11176.
19 K. Gong, F. Du, Z. Xia, M. Durstock and L. Dai, Nitrogen-Doped Carbon Nanotube Arrays with High Electrocatalytic Activity for Oxygen Reduction, *Science*, 2009, **323**(5915), 760–764.
20 L. Lai, J. R. Potts, D. Zhan, L. Wang, C. K. Poh, C. Tang, H. Gong, Z. Shen, J. Lin and R. S. Ruoff, Exploration of the Active Center Structure of Nitrogen-Doped Graphene-Based Catalysts for Oxygen Reduction Reaction, *Energy Environ. Sci.*, 2012, **5**(7), 7936–7942.
21 H. S. Kim, H. S. Kim, S. S. Kim and Y.-H. Kim, Atomistic Mechanisms of Codoping-Induced p-to n-Type Conversion in Nitrogen-Doped Graphene, *Nanoscale*, 2014, **6**(24), 14911–14918.
22 D. Usachov, O. Vilkov, A. Gruneis, D. Haberer, A. Fedorov, V. Adamchuk, A. Preobrajenski, P. Dudin, A. Barinov and M. Oehzelt, Nitrogen-Doped Graphene: Efficient Growth, Structure, and Electronic Properties, *Nano Lett.*, 2011, **11**(12), 5401–5407.
23 T. Schiros, D. Nordlund, L. Pálová, D. Prezzi, L. Zhao, K. S. Kim, U. Wurstbauer, C. Gutiérrez, D. Delongchamp and C. Jaye, Connecting Dopant Bond Type with Electronic Structure in N-Doped Graphene, *Nano Lett.*, 2012, **12**(8), 4025–4031.
24 W. J. Lee, U. N. Maiti, J. M. Lee, J. Lim, T. H. Han and S. O. Kim, Nitrogen-Doped Carbon Nanotubes and Graphene Composite Structures for Energy and Catalytic Applications, *Chem. Commun.*, 2014, **50**(52), 6818–6830.
25 M. Fan, C. Zhu, L. Liu, Q. Wu, Q. Hao, J. Yang and D. Sun, Modified PEDOT by Benign Preparing N-Doped Reduced Graphene Oxide as Potential Bio-Electrode Coating Material, *Green Chem.*, 2016, **18**(6), 1731–1737.
26 M. Guo, D. Li, M. Zhao, Y. Zhang, D. Geng, A. Lushington and X. Sun, Nitrogen Ion Implanted Graphene as Thrombo-Protective Safer and Cytoprotective Alternative for Biomedical Applications, *Carbon*, 2013, **61**, 321–328.
27 S. Boncel, K. H. Müller, J. N. Skepper, K. Z. Walczak and K. K. Koziol, Tunable Chemistry and Morphology of Multi-

Wall Carbon Nanotubes as a Route to Non-Toxic, Theranostic Systems, *Biomaterials*, 2011, **32**(30), 7677–7686.
28 Y. Yang, J. Zhang, J. Zhuang and X. Wang, Synthesis of Nitrogen-Doped Carbon Nanostructures from Polyurethane Sponge for Bioimaging and Catalysis, *Nanoscale*, 2015, **7**(29), 12284–12290.
29 M. Zhao, Y. Cao, X. Liu, J. Deng, D. Li and H. Gu, Effect of Nitrogen Atomic Percentage on N+-Bombarded MWCNTs in Cytocompatibility and Hemocompatibility, *Nanoscale Res. Lett.*, 2014, **9**(1), 142.
30 J. Carrero-Sanchez, A. Elias, R. Mancilla, G. Arrellin, H. Terrones, J. Laclette and M. Terrones, Biocompatibility and Toxicological Studies of Carbon Nanotubes Doped with Nitrogen, *Nano Lett.*, 2006, **6**(8), 1609–1616.
31 M. Zhao, D. Li, L. Yuan, Y. Yue, H. Liu and X. Sun, Differences in Cytocompatibility and Hemocompatibility between Carbon Nanotubes and Nitrogen-Doped Carbon Nanotubes, *Carbon*, 2011, **49**(9), 3125–3133.
32 A. L. Elías, J. C. Carrero-Sánchez, H. Terrones, M. Endo, J. P. Laclette and M. Terrones, Viability Studies of Pure Carbon- and Nitrogen-Doped Nanotubes with Entamoeba Histolytica: From Amoebicidal to Biocompatible Structures, *Small*, 2007, **3**(10), 1723–1729.
33 T. Okada, K. Y. Inoue, G. Kalita, M. Tanemura, T. Matsue, M. Meyyappan and S. Samukawa, Bonding State and Defects of Nitrogen-Doped Graphene in Oxygen Reduction Reaction, *Chem. Phys. Lett.*, 2016, **665**, 117–120.
34 Y. Liu, J. Li, W. Li, Y. Li, F. Zhan, H. Tang and Q. Chen, Exploring the Nitrogen Species of Nitrogen Doped Graphene as Electrocatalysts for Oxygen Reduction Reaction in Al–Air Batteries, *Int. J. Hydrogen Energy*, 2016, **41**(24), 10354–10365.
35 H. Miao, S. Li, Z. Wang, S. Sun, M. Kuang, Z. Liu and J. Yuan, Enhancing the Pyridinic N Content of Nitrogen-Doped Graphene and Improving Its Catalytic Activity for Oxygen Reduction Reaction, *Int. J. Hydrogen Energy*, 2017, **42**(47), 28298–28308.
36 T. Xing, Y. Zheng, L. H. Li, B. C. Cowie, D. Gunzelmann, S. Z. Qiao, S. Huang and Y. Chen, Observation of Active Sites for Oxygen Reduction Reaction on Nitrogen-Doped Multilayer Graphene, *ACS Nano*, 2014, **8**(7), 6856–6862.
37 H. B. Yang, J. Miao, S.-F. Hung, J. Chen, H. B. Tao, X. Wang, L. Zhang, R. Chen, J. Gao and H. M. Chen, Identification of Catalytic Sites for Oxygen Reduction and Oxygen Evolution in N-Doped Graphene Materials: Development of Highly Efficient Metal-Free Bifunctional Electrocatalyst, *Sci. Adv.*, 2016, **2**(4), e1501122.
38 Z.-H. Sheng, L. Shao, J.-J. Chen, W.-J. Bao, F.-B. Wang and X.-H. Xia, Catalyst-free Synthesis of Nitrogen-Doped Graphene via Thermal Annealing Graphite Oxide with Melamine and Its Excellent Electrocatalysis, *ACS Nano*, 2011, **5**(6), 4350–4358.
39 L. M. Gilbertson, E. M. Albalghiti, Z. S. Fishman, F. Perreault, C. Corredor, J. D. Posner, M. Elimelech, L. D. Pfefferle and J. B. Zimmerman, Shape-Dependent Surface Reactivity and Antimicrobial Activity of Nano-Cupric Oxide, *Environ. Sci. Technol.*, 2016, **50**(7), 3975–3984.
40 F. Perreault, A. F. de Faria, S. Nejati and M. Elimelech, Antimicrobial Properties of Graphene Oxide Nanosheets: Why Size Matters, *ACS Nano*, 2015, **9**(7), 7226–7236.
41 A. F. Faria, F. Perreault and M. Elimelech, Elucidating the Role of Oxidative Debris in the Antimicrobial Properties of Graphene Oxide, *ACS Appl. Nano Mater.*, 2018, **1**(3), 1164–1174.
42 X. Lu, X. Feng, J. R. Werber, C. Chu, I. Zucker, J.-H. Kim, C. O. Osuji and M. Elimelech, Enhanced Antibacterial Activity through the Controlled Alignment of Graphene Oxide Nanosheets, *Proc. Natl. Acad. Sci. U. S. A.*, 2017, **114**(46), E9793–E9801.
43 O. Akhavan, E. Ghaderi and A. Esfandiar, Wrapping Bacteria by Graphene Nanosheets for Isolation from Environment, Reactivation by Sonication, and Inactivation by Near-Infrared Irradiation, *J. Phys. Chem. B*, 2011, **115**(19), 6279–6288.
44 S. Liu, M. Hu, T. H. Zeng, R. Wu, R. Jiang, J. Wei, L. Wang, J. Kong and Y. Chen, Lateral Dimension-Dependent Antibacterial Activity of Graphene Oxide Sheets, *Langmuir*, 2012, **28**(33), 12364–12372.
45 H.-L. Guo, P. Su, X. Kang and S.-K. Ning, Synthesis and Characterization of Nitrogen-Doped Graphene Hydrogels by Hydrothermal Route with Urea as Reducing-Doping Agents, *J. Mater. Chem. A*, 2013, **1**(6), 2248–2255.
46 L. Sun, L. Wang, C. Tian, T. Tan, Y. Xie, K. Shi, M. Li and H. Fu, Nitrogen-Doped Graphene with High Nitrogen Level via a One-Step Hydrothermal Reaction of Graphene Oxide with Urea for Superior Capacitive Energy Storage, *RSC Adv.*, 2012, **2**(10), 4498–4506.
47 L. T. Soo, K. S. Loh, A. B. Mohamad, W. R. W. Daud and W. Y. Wong, Effect of Nitrogen Precursors on the Electrochemical Performance of Nitrogen-Doped Reduced Graphene Oxide towards Oxygen Reduction Reaction, *J. Alloys Compd.*, 2016, **677**, 112–120.
48 S. Kundu, T. C. Nagaiah, W. Xia, Y. Wang, S. V. Dommele, J. H. Bitter, M. Santa, G. Grundmeier, M. Bron, W. Schuhmann and M. Muhler, Electrocatalytic Activity and Stability of Nitrogen-Containing Carbon Nanotubes in the Oxygen Reduction Reaction, *J. Phys. Chem. C*, 2009, **113**(32), 14302–14310.
49 D. Wei, Y. Liu, Y. Wang, H. Zhang, L. Huang and G. Yu, Synthesis of N-Doped Graphene by Chemical Vapor Deposition and Its Electrical Properties, *Nano Lett.*, 2009, **9**(5), 1752–1758.
50 Z. Lin, G. Waller, Y. Liu, M. Liu and C. P. Wong, Facile Synthesis of Nitrogen-Doped Graphene via Pyrolysis of Graphene Oxide and Urea, and Its Electrocatalytic Activity toward the Oxygen-Reduction Reaction, *Adv. Energy Mater.*, 2012, **2**(7), 884–888.
51 A. C. Ferrari, J. C. Meyer, V. Scardaci, C. Casiraghi, M. Lazzeri, F. Mauri, S. Piscanec, D. Jiang, K. S. Novoselov, S. Roth and A. K. Geim, Raman Spectrum of Graphene and Graphene Layers, *Phys. Rev. Lett.*, 2006, **97**(18), 187401.
52 Z. Zafar, Z. H. Ni, X. Wu, Z. X. Shi, H. Y. Nan, J. Bai and L. T. Sun, Evolution of Raman Spectra in Nitrogen Doped Graphene, *Carbon*, 2013, **61**, 57–62.

53 A. C. Ferrari and J. Robertson, Interpretation of Raman Spectra of Disordered and Amorphous Carbon, *Phys. Rev. B: Condens. Matter Mater. Phys.*, 2000, **61**(20), 14095.

54 L. G. Cançado, A. Jorio, E. M. Ferreira, F. Stavale, C. Achete, R. Capaz, M. Moutinho, A. Lombardo, T. Kulmala and A. Ferrari, Quantifying Defects in Graphene via Raman Spectroscopy at Different Excitation Energies, *Nano Lett.*, 2011, **11**(8), 3190–3196.

55 L. Panchakarla, K. Subrahmanyam, S. Saha, A. Govindaraj, H. Krishnamurthy, U. Waghmare and C. Rao, Synthesis, Structure, and Properties of Boron-and Nitrogen-Doped Graphene, *Adv. Mater.*, 2009, **21**(46), 4726–4730.

56 S. Liu, T. H. Zeng, M. Hofmann, E. Burcombe, J. Wei, R. Jiang, J. Kong and Y. Chen, Antibacterial Activity of Graphite, Graphite Oxide, Graphene Oxide, and Reduced Graphene Oxide: Membrane and Oxidative Stress, *ACS Nano*, 2011, **5**(9), 6971–6980.

57 F. Perreault, A. Fonseca de Faria and M. Elimelech, Environmental Applications of Graphene-Based Nanomaterials, *Chem. Soc. Rev.*, 2015, **44**(16), 5861–5896.

58 X. Liu, S. Sen, J. Liu, I. Kulaots, D. Geohegan, A. Kane, A. A. Puretzky, C. M. Rouleau, K. L. More and G. T. R. Palmore, Antioxidant Deactivation on Graphenic Nanocarbon Surfaces, *Small*, 2011, **7**(19), 2775–2785.

59 X. Zou, L. Zhang, Z. Wang and Y. Luo, Mechanisms of the Antimicrobial Activities of Graphene Materials, *J. Am. Chem. Soc.*, 2016, **138**(7), 2064–2077.

60 C. Wu, C. Wang, J. Zheng, C. Luo, Y. Li, S. Guo and J. Zhang, Vacuolization in Cytoplasm and Cell Membrane Permeability Enhancement Triggered by Micrometer-Sized Graphene Oxide, *ACS Nano*, 2015, **9**(8), 7913–7924.

61 Y. Tu, M. Lv, P. Xiu, T. Huynh, M. Zhang, M. Castelli, Z. Liu, Q. Huang, C. Fan and H. Fang, Destructive Extraction of Phospholipids from Escherichia Coli Membranes by Graphene Nanosheets, *Nat. Nanotechnol.*, 2013, **8**(8), 594.

62 D. P. Jones, Redox Potential of GSH/GSSG Couple: Assay and Biological Significance, in *Methods Enzymol.*, Elsevier, 2002, vol. 348, pp. 93–112.

63 G. Smirnova, N. Muzyka and O. Oktyabrsky, Transmembrane Glutathione Cycling in Growing Escherichia Coli Cells, *Microbiol. Res.*, 2012, **167**(3), 166–172.

64 R. A. Owensm and P. E. Hartman, Glutathione: a Protective Agent in Salmonella Typhimurium and Escherichia Coli as Measured by Mutagenicity and by Growth Delay Assays, *Environ. Mutagen.*, 1986, **8**(5), 659–673.

65 F. Q. Schafer and G. R. Buettner, Redox Environment of the Cell as Viewed through the Redox State of the Glutathione Disulfide/Glutathione Couple, *Free Radical Biol. Med.*, 2001, **30**(11), 1191–1212.

66 R. Zhou, Y. Zheng, D. Hulicova-Jurcakova and S. Z. Qiao, Enhanced Electrochemical Catalytic Activity by Copper Oxide Grown on Nitrogen-Doped Reduced Graphene Oxide, *J. Mater. Chem. A*, 2013, **1**(42), 13179–13185.

67 Y. Liang, Y. Li, H. Wang, J. Zhou, J. Wang, T. Regier and H. Dai, Co3O4 Nanocrystals on Graphene as a Synergistic Catalyst for Oxygen Reduction Reaction, *Nat. Mater.*, 2011, **10**(10), 780–786.

68 Z.-J. Jiang and Z. Jiang, Interaction Induced High Catalytic Activities of CoO Nanoparticles Grown on Nitrogen-Doped Hollow Graphene Microspheres for Oxygen Reduction and Evolution Reactions, *Sci. Rep.*, 2016, **6**, 27081.

69 A. Bagri, C. Mattevi, M. Acik, Y. J. Chabal, M. Chhowalla and V. B. Shenoy, Structural Evolution during the Reduction of Chemically Derived Graphene Oxide, *Nat. Chem.*, 2010, **2**(7), 581–587.

70 C. Gómez-Navarro, J. C. Meyer, R. S. Sundaram, A. Chuvilin, S. Kurasch, M. Burghard, K. Kern and U. Kaiser, Atomic Structure of Reduced Graphene Oxide, *Nano Lett.*, 2010, **10**(4), 1144–1148.

71 Z. Luo, S. Lim, Z. Tian, J. Shang, L. Lai, B. MacDonald, C. Fu, Z. Shen, T. Yu and J. Lin, Pyridinic N Doped Graphene: Synthesis, Electronic Structure, and Electrocatalytic Property, *J. Mater. Chem.*, 2011, **21**(22), 8038–8044.

72 A. J. Bard and L. R. Faulkner, Methods Involving Forced Convection-Hydrodynamic Methods, in *Electrochemical Methods: Fundamentals and Applications*, Wiley, New York, 2nd edn, 2001, pp. 331–364.

73 X. Ge, A. Sumboja, D. Wuu, T. An, B. Li, F. W. T. Goh, T. S. A. Hor, Y. Zong and Z. Liu, Oxygen Reduction in Alkaline Media: From Mechanisms to Recent Advances of Catalysts, *ACS Catal.*, 2015, **5**(8), 4643–4667.

74 G. A. Ferrero, K. Preuss, A. Marinovic, A. B. Jorge, N. Mansor, D. J. L. Brett, A. B. Fuertes, M. Sevilla and M.-M. Titirici, Fe–N-Doped Carbon Capsules with Outstanding Electrochemical Performance and Stability for the Oxygen Reduction Reaction in Both Acid and Alkaline Conditions, *ACS Nano*, 2016, **10**(6), 5922–5932.

75 Y. Okamoto, First-Principles Molecular Dynamics Simulation of O2 Reduction on Nitrogen-Doped Carbon, *Appl. Surf. Sci.*, 2009, **256**(1), 335–341.

76 H. Niwa, K. Horiba, Y. Harada, M. Oshima, T. Ikeda, K. Terakura, J.-i. Ozaki and S. Miyata, X-Ray Absorption Analysis of Nitrogen Contribution to Oxygen Reduction Reaction in Carbon Alloy Cathode Catalysts for Polymer Electrolyte Fuel Cells, *J. Power Sources*, 2009, **187**(1), 93–97.

77 H. Kim, K. Lee, S. I. Woo and Y. Jung, On the Mechanism of Enhanced Oxygen Reduction Reaction in Nitrogen-Doped Graphene Nanoribbons, *Phys. Chem. Chem. Phys.*, 2011, **13**(39), 17505–17510.

78 I. C. Man, H. Y. Su, F. Calle-Vallejo, H. A. Hansen, J. I. Martínez, N. G. Inoglu, J. Kitchin, T. F. Jaramillo, J. K. Nørskov and J. Rossmeisl, Universality in Oxygen Evolution Electrocatalysis on Oxide Surfaces, *ChemCatChem*, 2011, **3**(7), 1159–1165.

79 M. J. McAllister, J.-L. Li, D. H. Adamson, H. C. Schniepp, A. A. Abdala, J. Liu, M. Herrera-Alonso, D. L. Milius, R. Car and R. K. Prud'homme, Single Sheet Functionalized Graphene by Oxidation and Thermal Expansion of Graphite, *Chem. Mater.*, 2007, **19**(18), 4396–4404.

80 J. E. Hutchison, Greener Nanoscience: A Proactive Approach to Advancing Applications and Reducing Implications of Nanotechnology, *ACS Nano*, 2008, **2**(3), 395–402.

